Journal of Solid State Chemistry 184 (2011) 675–683

Contents lists available at ScienceDirect

Journal of Solid State Chemistry

journal homepage: www.elsevier.com/locate/jssc

Synthesis, structures, luminescent and magnetic properties of four coordination polymers with the flexible 1,3-phenylenediacetate ligands

Jin-Zhong Gu [a,*], Dong-Yu Lv [a], Zhu-Qing Gao [b], Jian-Zhao Liu [a], Wei Dou [a], Yu Tang [a]

[a] Key Laboratory of Nonferrous Metal Chemistry and Resources Utilization of Gansu Province, College of Chemistry and Chemical Engineering, Lanzhou University, Lanzhou 730000, PR China

[b] School of Chemistry and Biology Engineering, Taiyuan University of Science and Technology, Taiyuan 030021, PR China

ARTICLE INFO

Article history:
Received 16 July 2010
Received in revised form
10 January 2011
Accepted 24 January 2011
Available online 1 February 2011

Keywords:
1,3-Phenylendiacetic acid
Coordination polymer
Photoluminescence
Magnetism

ABSTRACT

Four coordination polymers, $[Zn(pda)(bpy)(H_2O)]_n \cdot nH_2O$ (**1**), $[Cd(pda)(prz)(H_2O)]_n$ (**2**), $[Co_3(\mu_3\text{-}OH)_2(pda)_2(pyz)]_n \cdot 2nH_2O$ (**3**) and $[Pr_2(pda)_3(H_2O)_2]_n$ (**4**) (H_2pda = 1,3-phenylendiacetic acid, bpy = 4,4′-bipyridine, prz = piperazine and pyz = pyrazine) have been hydrothermally synthesized and characterized. Complex **1** is a 1D wheel-like chain structure, which is further extended into a 3D metal-organic supramolecular framework by H-bonds and π–π stacking interactions. Complex **2** is a 1D ladder-like chain structure, which is also further extended into a 3D metal-organic supramolecular framework by H-bonds. Complex **3** possess a 2D sheet structure with infrequent two pairs of double-helix chains. Complex **4** features a 3D structure. Both **1** and **2** display strong blue fluorescent emission at room temperature. Magnetic susceptibility measurements of complexes **3** and **4** exhibit antiferromagnetic interactions between the nearest metal ions, with C = 9.99 and 3.43 $cm^3\ mol^{-1}\ K$, and $\theta = -23.9$ and -46.3 K, respectively.

1. Introduction

The rational design and syntheses of coordination polymers have attracted great interests not only for their intriguing architectures and topologies but also for their potential applications in areas of catalysis, sorption, separation, luminescence, magnetism, nonlinear optical property, etc. [1–7]. One of the obvious challenges is the rational and controllable preparation of metal-organ frameworks, the formation of which is greatly affected by the organic ligands, the nature of the metal ions, counterions, pH values of the reaction solution, ancillary ligands and other factors [8–10]. The most effective and facile approach to overcome the problem is the appropriate choice of the well-designed organic bridging ligands containing modifiable backbones and connectively information, together with the metal centers with various coordination preferences. Many multi-carboxylate or heterocylic carboxylic acids are used for this purpose [11–13]. In order to extend the investigation in this field, we chose 1,3-phenylendiacetic acid as functional ligand, which is based on the following considerations: (1) comparing with isophthalate, it possess more flexible longer terminal groups ($-CH_2COO^-$ vs. $-COO^-$) in the same position. (2) It can act not only as hydrogen-bond acceptor but also as hydrogen-bond donor which depend upon the number of deprotonated carboxyl group, which is beneficial for the construction of coordination polymers.

Herein, we report the hydrothermal syntheses, crystal structures, photoluminescent and magnetic properties of four new coordination polymers $[Zn(pda)(bpy)(H_2O)]_n \cdot nH_2O$ (**1**), $[Cd(pda)(prz)(H_2O)]_n$ (**2**), $[Co_3(\mu_3\text{–}OH)_2(pda)_2(pyz)]_n \cdot 2nH_2O$ (**3**) and $[Pr_2(pda)_3(H_2O)_2]_n$ (**4**). Interestingly, by careful choice of the metal centers, pH values of the reaction solution and ancillary ligands, this series of polymeric networks exhibit varied structural features and binding modes of the pda ligands.

2. Experimental section

2.1. Materials and methods

All chemicals are commercially available and used without further purification. Elemental analyses were determined using Elementar Vario EL elemental analyzer. The IR spectra were recorded in the 4000–400 cm^{-1} region using KBr pellets and a Bruker VECTOR 22 spectrometer. Excitation and emission spectra were recorded on an Edinburgh FLS920 fluorescence spectrometer at room temperature for the solid samples. Thermogravimetric analysis (TG) data were collected on a Netzsch TG-209 instrument with a heating rate of 10 °C/min. X-ray powder diffraction (XRPD) measurements were recorded on a RIGAKU D/MAX 2200 VPC diffractometer. Magnetic susceptibility data were collected in the

* Corresponding author. Fax: +86 931 8915196.
E-mail address: gujzh@lzu.edu.cn (J.-Z. Gu).

0022-4596/$ - see front matter Crown Copyright © 2011 Published by Elsevier Inc. All rights reserved.
doi:10.1016/j.jssc.2011.01.030

2–300 K temperature range with a Quantum Design SQUID Magnetometer MPMS XL-7 and a field of 1000 Oe. A correction was made for the diamagnetic contribution prior to data analysis.

2.2. Synthesis of $[Zn(pda)(bpy)(H_2O)]_n \cdot nH_2O$ (**1**)

A mixture of $Zn(NO_3)_2 \cdot 6H_2O$ (0.090 g, 0.3 mmol), H_2pda (0.058 g, 0.3 mmol), NaOH (0.024 g, 0.6 mmol), 4,4′-bpy (0.047 g, 0.3 mmol) and H_2O (8 ml) was sealed in a 25 ml Teflon-lined stainless steel vessel, and heated at 160 °C for 3 days, followed by cooling to room temperature at a rate of 10 °C /h. Colorless block-shaped crystals of **1** were isolated in 70% yield (0.0944 g), and washed with distilled water. Anal. Calcd for $C_{20}H_{20}N_2O_6Zn$ (%): C 53.17, H 4.91, N 6.20. Found: C 53.56, H 4.68, N 5.96. IR data (KBr, cm^{-1}): 3421m, 2362w, 1605m, 1554vs, 1439m, 1390s, 1292m, 816m, 743s, 632m.

2.3. Synthesis of $[Cd(pda)(prz)(H_2O)]_n$ (**2**)

A mixture of $Cd(NO_3)_2 \cdot 4H_2O$ (0.0925 g, 0.3 mmol), H_2pda (0.058 g, 0.3 mmol), prz (0.078 g, 0.9 mmol) and H_2O (8 ml) was sealed in a 25 ml Teflon-lined stainless steel vessel, and heated at 160 °C for 3 days, followed by cooling to room temperature at a rate of 10 °C/h. Colorless block-shaped crystals of **2** were isolated in 60% yield (0.0658 g), and washed with distilled water. Anal. Calcd for $C_{12}H_{15}NO_5Cd$ (%): C 39.42, H 4.13, N 3.83. Found: C 39.86, H 3.88, N 4.16. IR data (KBr, cm^{-1}): 3390m, 3195s, 2363m, 1550vs, 1400s, 1278m, 1235w, 1090w, 996w, 944w, 875w, 727s.

2.4. Synthesis of $[Co_3(\mu_3\text{–}OH)_2(pda)_2(pyz)]_n \cdot 2nH_2O$ (**3**)

A mixture of $Co(NO_3)_2 \cdot 6H_2O$ (0.087 g, 0.3 mmol), H_2pda (0.058 g, 0.3 mmol), pyz (0.024 g, 0.3 mmol), NaOH (0.024 g, 0.6 mmol) and H_2O–CH_3OH (10 ml, v:v=5:1) was sealed in a 25 ml Teflon-lined stainless steel vessel, and heated at 160 °C for 3 days, followed by cooling to room temperature at a rate of 10 °C/h. Purple needle-shaped crystals of **3** were isolated in 65% yield (0.046 g), and washed with distilled water. Anal. Calcd for $C_{24}H_{26}N_2O_{12}Co_3$ (%): C 40.53, H 3.68, N 3.94. Found: C 40.26, H 3.98, N 4.27. IR data (KBr, cm^{-1}): 3407s, 1595w, 1575vs, 1418m, 1394w, 1276w, 1056w, 818w, 718m.

2.5. Synthesis of $[Pr_2(pda)_3(H_2O)_2]_n$ (**4**)

A mixture of $Pr(NO_3)_2 \cdot 6H_2O$ (0.087 g, 0.2 mmol), H_2pda (0.058 g, 0.3 mmol), a drop of triethylamine and H_2O (8 ml) was sealed in a 25 ml Teflon-lined stainless steel vessel, and heated at 160 °C for 3 days, followed by cooling to room temperature at a rate of 10 °C/h. Yellow block-shaped crystals of **4** were isolated in 72% yield (0.064 g), and washed with distilled water. Anal. Calcd for $C_{30}H_{28}O_{14}Pr_2$ (%): C 40.29, H 3.16. Found: C 40.67, H 3.48. IR data (KBr, cm^{-1}): 3425s, 1542vs, 1407vs, 1273m, 1154w, 941w, 724m.

3. X-ray crystallography

Single-crystal data for **1**–**4** were collected at 296(2) K on a Bruker Smart 1000 CCD diffractometer with Mo $K\alpha$ radiation (λ=0.71073 Å). All empirical absorption corrections were applied by using the SADABS program [14]. The structures were solved using direct method, which yielded the positions of all non-hydrogen atoms. These were first refined isotropically and then anisotropically. All the hydrogen atoms (except the ones bound to water molecules) were placed in calculated positions with fixed isotropic thermal parameters and included in structure factor calculations in the final stage of full-matrix least-squares refinement. The hydrogen atoms of water molecules in **1**–**4** were located in the difference Fourier map and refined isotropically. All calculations were performed using the SHELXTL-97 system of computer programs [15]. The crystallographic data are summarized in Table 1. The selected bond lengths and angles are listed in Table 2.

Table 1
The crystallographic data for **1**–**4**.

Compound	**1**	**2**	**3**	**4**
Formula	$C_{20}H_{20}N_2O_6Zn$	$C_{12}H_{15}NO_5Cd$	$C_{24}H_{26}N_2O_{12}Co_3$	$C_{30}H_{28}O_{14}Pr_2$
fw	449.75	365.65	711.26	894.34
Crystal size (mm)	0.22 × 0.20 × 0.16	0.22 × 0.20 × 0.18	0.22 × 0.21 × 0.20	0.20 × 0.18 × 0.14
Cryst syst	*Triclinic*	*Triclinic*	*Monoclinic*	*Triclinic*
Space group	*P*-1	*P*-1	*P*2/c	*P*-1
a/Å	8.3196(14)	5.9591(11)	23.315(3)	10.5225(2)
b/Å	11.3917(17)	9.846(2)	9.7287(13)	12.0132(2)
c/Å	11.4516(17)	11.761(2)	11.8332(16)	12.4160(2)
α/°	67.848(8)	101.276(8)	90	105.6860(10)
β/°	87.092(9)	104.021(8)	104.487(7)	97.0290(10)
γ/°	68.592(8)	95.852(8)	90	92.7630(10)
vol/Å^3	931.1(3)	648.4(2)	2598.7(6)	1494.25(4)
Z	2	2	4	2
D_C/Mg m^{-3}	1.604	1.873	1.818	1.988
F(0 0 0)	464	364	1444	876
μ/mm^{-1}	1.361	1.699	1.963	3.295
θ (deg.)	2.08–25.29	1.83–25.10	0.90–25.10	1.72–26.00
Reflns collected	4845	3400	13177	8445
Unique reflns (*R*int)	3321 (0.0353)	2281 (0.0104)	4620 (0.0377)	5777 (0.0163)
Parameters	264	180	371	415
$\Delta(\rho)$(e Å^{-3})	0.642, −0.971	0.258, −0.464	1.806, −0.405	0.673, −0.643
S on F^2	1.032	1.042	1.064	1.026
R_1[a], wR_2[b] [$I > 2\sigma(I)$]	0.0589, 0.1538	0.0186, 0.0478	0.0427, 0.0997	0.0245, 0.0531
R_1[a], wR_2[b] (all data)	0.0774, 0.1702	0.0192, 0.0484	0.0558, 0.1063	0.0312, 0.0561

Weighting: **1**, $w=1/[\sigma^2(F_o)^2+(0.0963P)^2+0.000P]$; **2**, $w=1/[\sigma^2(F_o)^2+(0.0^256P)^2+0.464P]$; **3**, $w=1/[\sigma^2(F_o)^2+(0.0560P)^2+1.087P]$; **4**, $w=1/[\sigma^2(F_o)^2+(0.0239P)^2+0.6684P]$.

[a] $R_1=\Sigma||F_o|-|F_c||/\Sigma|F_o|$.

[b] $wR_2=[\Sigma[w(F_o^2-F_c^2)^2]/\Sigma w(F_o^2)^2]^{1/2}$.

Table 2
Selected bond distances (Å) and bond angles (deg.) for compounds **1–4**.

Complex **1**					
Zn(1)–O(2)#1	2.027(4)	Zn(1)–O(5)	2.094(4)	Zn(1)–O(4)	2.163(3)
Zn(1)–O(3)	2.292(4)	Zn(1)–N(1)	2.149(4)	Zn(1)–N(2)#2	2.189(4)
O(2)#1–Zn(1)–O(5)	101.48(16)	O(2)#1–Zn(1)–N(1)	94.64(14)	O(5)–Zn(1)–N(1)	89.95(14)
O(2)#1–Zn(1)–O(4)	102.81(14)	O(5)–Zn(1)–O(4)	155.27(15)	N(1)–Zn(1)–O(4)	92.66(14)
O(2)#1–Zn(1)–N(2)#2	88.42(15)	O(5)–Zn(1)–N(2)#2	89.54(14)	N(1)–Zn(1)–N(2)#2	176.94(15)
O(4)–Zn(1)–N(2)#2	86.55(14)	O(2)#1–Zn(1)–O(3)	160.29(14)	O(5)–Zn(1)–O(3)	96.78(14)
N(1)–Zn(1)–O(3)	92.73(14)	O(4)–Zn(1)–O(3)	58.54(12)	N(2)#2–Zn(1)–O(3)	84.34(14)
Complex **2**					
Cd(1)–O(5)	2.2529(19)	Cd(1)–O(4)	2.2728(17)	Cd(1)–O(2)#1	2.275(2)
Cd(1)–N(1)	2.2887(19)	Cd(1)–O(1)#1	2.4252(19)	Cd(1)–O(3)	2.4342(17)
O(5)–Cd(1)–O(4)	91.15(7)	O(5)–Cd(1)–O(2)#1	102.10(9)	O(4)–Cd(1)–O(2)#1	144.23(7)
O(5)–Cd(1)–N(1)	90.31(8)	O(4)–Cd(1)–N(1)	119.35(7)	O(2)#1–Cd(1)–N(1)	93.94(7)
O(5)–Cd(1)–O(1)#1	104.63(9)	O(4)–Cd(1)–O(1)#1	89.91(7)	O(2)#1–Cd(1)–O(1)#1	54.73(7)
N(1)–Cd(1)–O(1)#1	147.16(7)	O(5)–Cd(1)–O(3)	145.33(7)	O(4)–Cd(1)–O(3)	55.41(6)
O(2)#1–Cd(1)–O(3)	110.66(8)	N(1)–Cd(1)–O(3)	98.27(6)	O(1)#1–Cd(1)–O(3)	85.96(7)
Complex **3**					
Co(1)–O(5)#1	2.047(2)	Co(1)–O(1)	2.080(3)	Co(1)–O(3)#2	2.081(3)
Co(1)–O(5)	2.098(2)	Co(1)–N(2)	2.193(3)	Co(1)–O(4)#3	2.204(3)
Co(2)–O(2)#4	2.073(3)	Co(2)–O(2)#5	2.073(3)	Co(2)–O(5)#3	2.099(2)
Co(2)–O(5)#6	2.099(2)	Co(2)–O(4)	2.183(3)	Co(2)–O(4)#7	2.183(3)
O(5)–Co(1)#1	2.047(2)	O(5)#1–Co(1)–O(1)	97.55(10)	O(5)#1–Co(1)–O(3)#2	176.63(11)
O(1)–Co(1)–O(3)#2	80.87(11)	O(5)#1–Co(1)–O(5)	85.66(10)	O(1)–Co(1)–O(5)	95.18(10)
O(3)#2–Co(1)–O(5)	91.50(10)	O(5)#1–Co(1)–N(2)	97.90(11)	O(1)–Co(1)–N(2)	89.08(12)
O(3)#2–Co(1)–N(2)	85.08(11)	O(5)–Co(1)–N(2)	174.06(11)	O(5)#1–Co(1)–O(4)#3	90.13(10)
O(1)–Co(1)–O(4)#3	167.47(10)	O(3)#2–Co(1)–O(4)#3	90.92(10)	O(5)–Co(1)–O(4)#3	75.47(10)
N(2)–Co(1)–O(4)#3	99.68(11)	O(2)#4–Co(2)–O(2)#5	93.37(16)	O(2)#4–Co(2)–O(5)#3	86.59(10)
O(2)#5–Co(2)–O(5)#3	94.58(10)	O(2)#4–Co(2)–O(5)#6	94.58(10)	O(2)#5–Co(2)–O(5)#6	86.59(10)
O(5)#3–Co(2)–O(5)#6	178.30(14)	O(2)#4–Co(2)–O(4)	161.94(10)	O(2)#5–Co(2)–O(4)	92.36(10)
O(5)#3–Co(2)–O(4)	75.88(9)	O(5)#6–Co(2)–O(4)	102.85(10)	O(2)#4–Co(2)–O(4)#7	92.36(10)
O(2)#5–Co(2)–O(4)#7	161.94(10)	O(5)#3–Co(2)–O(4)#7	102.85(10)	O(5)#6–Co(2)–O(4)#7	75.88(9)
O(4)–Co(2)–O(4)#7	87.40(14)	Co(1)#1–O(5)–Co(1)	94.34(10)	Co(1)#1–O(5)–Co(2)#3	119.52(12)
Co(1)–O(5)–Co(2)#3	99.70(10)				
Complex **4**					
Pr(1)–O(1)#1	2.426(2)	Pr(1)–O(7)#2	2.431(2)	Pr(1)–O(3)	2.459(2)
Pr(1)–O(8)#3	2.462(3)	Pr(1)–O(12)#4	2.515(3)	Pr(1)–O(13)	2.536(3)
Pr(1)–O(6)	2.540(2)	Pr(1)–O(5)	2.600(3)	Pr(1)–O(7)#3	2.756(3)
Pr(2)–O(4)#5	2.394(3)	Pr(2)–O(11)#4	2.447(2)	Pr(2)–O(9)#6	2.480(2)
Pr(2)–O(5)	2.492(2)	Pr(2)–O(14)	2.546(3)	Pr(2)–O(2)#1	2.548(3)
Pr(2)–O(10)	2.567(3)	Pr(2)–O(1)#1	2.592(2)	Pr(2)–O(9)	2.626(2)
Pr(1)#1–O(1)–Pr(2)#1	111.56(8)	Pr(2)–O(5)–Pr(1)	109.20(9)		

Symmetry transformations used to generate equivalent atoms: #1 $-x+1, -y+2, -z+2$, #2 $x, y+1, z$, for **1**; #1 $x, y+1, z$, for **2**; #1 $-x, -y+1, -z+1$, #2 $x, -y, z+1/2$, #3 $-x, -y, -z+1$, #4 $-x, y-1, -z+1/2$, #5 $x, y-1, z$, #6 $x, -y, z-1/2$, #7 $-x, y, -z+1/2$, for **3**; #1 $-x+2, -y+1, -z+2$, #2 $-x+2, -y+3, -z+3$, #3 $x, y-1, z$, #4 $x, y, z+1$, #5 $-x+2, -y+2, -z+2$, for **4**.

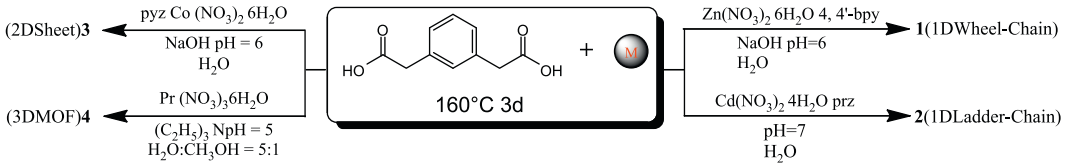

Scheme 1. The synthetic routes for complexes **1–4**.

4. Results and discussion

4.1. Syntheses

Compounds **1–4** were obtained by hydrothermal reactions (Scheme 1). The pH values of the solution were 6, 7, 6 and 5, respectively. Three kinds of bases were used for adjusting the pH values of the solution, NaOH for **1** and **3**, prz for **2**, triethylamine for **4**, respectively. Complexes **1–4** with different structural features were obtained by using different metal ions and ancillary ligands (4,4′-bpy, prz and pyz) at the same reaction temperatures. Obviously, metal ions and the ancillary ligands play important roles in resulting products for this system.

4.2. Crystal structures

4.2.1. $[Zn(pda)(bpy)H_2O]_n \cdot H_2O$ (**1**)

Crystallographic analysis reveals that complex **1** crystallizes in the triclinic space group $P-1$. The Zn1 center is six-coordinated with a distorted octahedral geometry, which three O (O3, O4, and O2i) atoms from two individual pda ligands and one O (O5) atom from one coordinated water molecule occupy the equatorial positions, and two N (N1 and N2ii) atoms from two individual 4,4′-bpy auxiliary ligands occupy the axial positions (Fig. 1). The Zn–O and Zn–N distances are 2.027(4)–2.292(4) and 2.149(4)–2.189(4) Å, respectively. The pda ligand adopts μ_2-tridentate coordination mode (Scheme 2(a)). In **1**, two Zn(II) ions and two

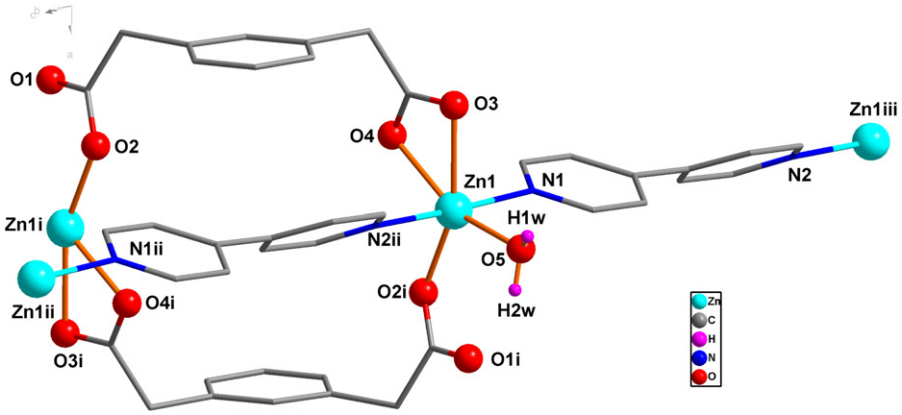

Fig. 1. The coordination environments of Zn^{2+}, pda, and 4,4′-bpy in **1**.

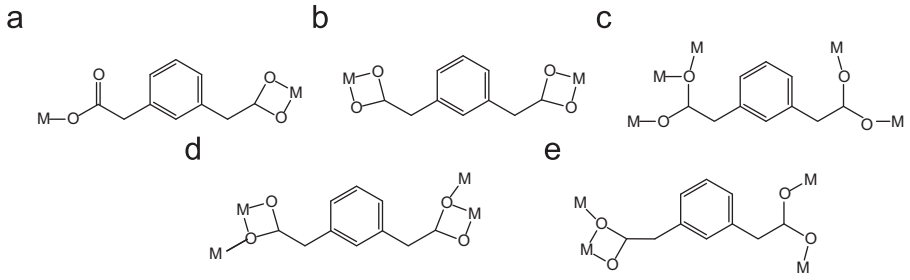

Scheme 2. Coordination modes of the pda^{2-} ligands in complexes **1–4**.

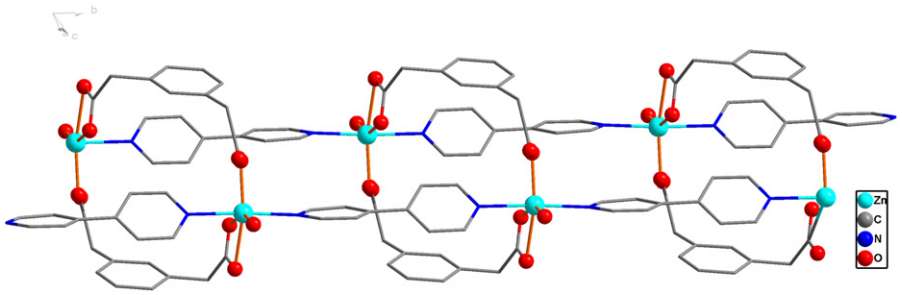

Fig. 2. 1D wheel-like chain structure along *a* axis in **1**.

pda ligands form a $[Zn_2(pda)_2]$ ring. The Zn…Zn distance is 7.9498(2) Å in the ring. The rings are further connected by the coordination interactions of the 4,4′-bpy auxiliary ligands to generate a 1D wheel-like chain structure (Fig. 2), which is further extended into a 3D metal-organic supramolecular framework by H-bonds and π–π stacking interactions with the centroid–centroid distance of 3.999(3) Å (Figs. S1, S2 and Table 3).

4.2.2. $[Cd(pda)(prz)H_2O]_n$ (**2**)

As shown in Fig. 3, Cd1 ion is also six-coordinated in a distorted octahedral geometry with three O atoms (O2i, O3 and O4) from two individual pda ligands and one O (O5) atom from one coordinated water molecule occupy the equatorial positions, and one N (N1) atom from prz auxiliary ligand and one O atom (O1i) from the carboxyl group of the pda occupy the axial positions. The Cd–O and Cd–N distances are 2.2529(2)–2.4342(2) and 2.2887(2) Å, respectively. The pda ligand adopts μ_2-quadridentate coordination mode (Scheme 2(b)). Pda ligand bridges the two adjacent Cd(II) ions through its two chelating carboxylate groups to form infinite helical chains (Fig. 4). The distance of the two adjacent Cd ions is 9.846(2) Å in the chain. The two adjacent helical chains are further connected by the coordination interactions of the prz ligands to form a 1D ladder-like chain, which is further extended into a 3D metal-organic supramolecular framework by H-bonds and π–π stacking interactions inter-chains (Figs. S3, S4, and Table 3).

4.2.3. $[Co_3(\mu_3\text{–}OH)_2(pda)_2(pyz)]_n \cdot 2H_2O$ (**3**)

The X-ray structure analysis of **3** reveals that there are two independent $[Co_{1.5}(\mu_3\text{–}OH)(pda)(pyz)_{0.5}]\cdot H_2O$ molecules in one asymmetric unit, and the compound crystallizes in the monoclinic space group *P*2/*c*. Two $[Co_{1.5}(\mu_3\text{–}OH)(pda)(pyz)_{0.5}]\cdot H_2O$ molecules have the same structures, thus the one involving Co1 and Co2 atoms is described in details here. Co1 ion is six-coordinated in a distorted octahedral geometry with two O atoms (O1 and O4iii) from two individual pda ligands, one O (O5) atom

Table 3
Hydrogen bond lengths (Å) and bond angles (deg.).

D–H···A	D–H	H···A	D···A	∠DHA	Symmetry code
Complex **1**					
O(5)–H(2W)…O(1)	0.851(19)	1.86(3)	2.624(6)	148(5)	
O(5)–H(1W)…O(3)	0.853(19)	1.861(19)	2.712(5)	175(5)	
Complex **2**					
O(5)–H(1W)…O(4)	0.854(17)	1.824(18)	2.676(3)	176(3)	$-x, -y+1, -z+1$
O(5)–H(2W)…O(1)	0.849(17)	1.951(18)	2.796(3)	173(3)	$x-1, y+1, z$
N(1)–H(1)…O(3)	0.91	2.18	3.068(3)	164.3	$x-1, y, z$
Complex **3**					
O(5)–H(1W)…O(12)	0.94	2.64	3.273(5)	125.4	
O(10)–H(2W)…O(11)	0.96	2.57	3.316(5)	134.7	$x, y-1, z$
O(11)–H(3W)…O(6)	0.87	2.04	2.874(5)	161.7	$x, y+1, z$
O(11)–H(3W)…O(8)	0.87	2.64	3.261(5)	129.6	$x, -y+2, z+1/2$
O(12)–H(6W)…O(1)	0.87	2.09	2.884(5)	151.3	
O(12)–H(6W)…O(3)	0.87	2.56	3.249(5)	137.3	$x, -y, z+1/2$
Complex **4**					
O(13)–H(2W)…O(12)	0.86	2.00	2.856(4)	179.4	$-x+2, -y+2, -z+2$
O(14)–H(4W)…O(3)	0.91	2.73	2.847(4)	88.0	$-x+2, -y+2, -z+2$
O(14)–H(3W)…O(14)	0.90	2.50	3.084(5)	122.5	$-x+2, -y+2, -z+2$
O(14)–H(4W)…O(6)	0.91	2.36	3.184(4)	150.5	$-x+2, -y+2, -z+2$

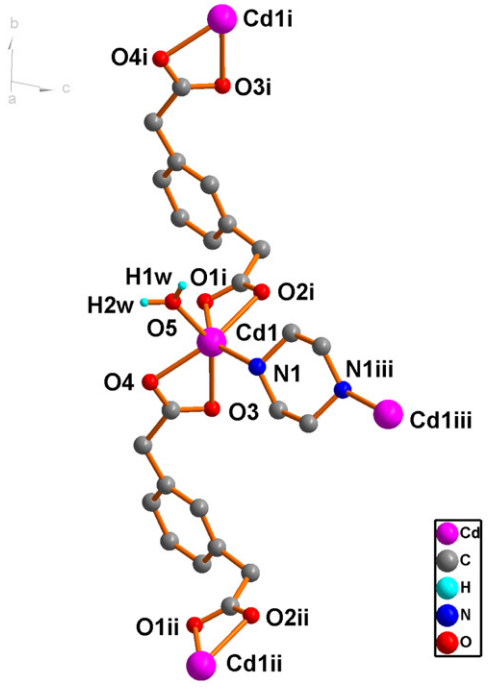

Fig. 3. The coordination environments of Cd^{2+}, pda, and prz in **2** (symmetry code: i, $x, y+1, z$; ii, $x, y-1, z$; iii, $-x, -y+1, -z+2$).

from μ_3–OH group, and one N atom (N2) from the pyz ligand occupy the equatorial positions and one O (O5i) atom from the carboxylate group of pda ligand and one O atom (O3ii) from μ_3–OH group occupy the axial positions (Fig. 5). Co2 ion is also six-coordinated in a distorted octahedral geometry, in which four O atoms (O2iv, O2v, O4 and O4vii) from four individual pda ligands occupy the equatorial positions and two O (O5iii and O5vi) atoms from two individual μ_3–OH groups occupy the axial positions. The Co–O and Co–N distances are 2.047(2)–2.204(3) and 2.193(3) Å, respectively. Each μ_3–OH^- anion bridges three Co(II) ions, with the distances and angles of 2.047(2)–2.099(2) Å and 94.34(10), 99.70(10) and 119.52(12)°, respectively. Each pda ligand takes μ_5-pentadentate coordination mode (Scheme 1(c)).

Pda ligands and μ_3–OH^- groups bridge the Co(II) centers to form infrequent two pairs of double-helix chains (Fig. 6). Then the chains are further extended into 2D sheet by the coordinated interaction of pda ligands and pyz ligands (Fig. 7). Finally, 3D supramolecular framework is formed by H-bonds interactions inter-layers (Figs. S5, S6 and Table 3).

4.2.4. $[Pr_2(pda)_3(H_2O)_2]_n$ (**4**)

X-ray crystallography reveals that complex **4** crystallizes in the triclinic space group $P-1$. Each asymmetric unit of **4** contains two crystallographically unique Pr(III) ions, three pda ligands and two coordinated water molecules (Fig. 8). Both Pr1 and Pr2 are nine-coordinated with a distorted tricapped trigonal prism geometry. The nine coordination sites are occupied by an aqua oxygen atom and eight O atoms from six different pda ligands. The Pr–O distances are 2.394(3)–2.756(3) Å. All the M–O and M–N distances in compounds **1**–**4** are comparable to those reported for other M–O and M–O donor complexes [16–19].

The pda ligands adopt two coordination modes (μ_4-hexadentate and μ_4-pentadentate), as shown in Scheme 2(d) and (e). As shown in Fig. 9, eight Pr(III) ions and 12 pda ligands form a large $[Pr_8(pda)_{12}]$ ring, and four Pr(III) ions and six pda^{2-} ligands form a small $[Pr_4(pda)_6]$ ring. The rings are further connected by the coordination interactions of pda ligands and Pr(III) to generate a 3D MOF, as shown in Fig. 10.

4.2.5. *The coordination modes of pda^{2-} ligands in complexes* ***1*–*4***

In complexes **1**–**4**, pda ligands take five different kinds of coordination modes (Scheme 2). In **1**, the pda ligand adopts a μ_2-bridging mode with one carboxylate group in a $\mu_1\_\eta^1$: η^1 chelating mode and the other in a $\mu_1\_\eta^1$: η^0 monodentate mode (Scheme 2(a)) [17]. In **2**, the pda ligand takes a μ_2-bridging mode with two carboxylate groups in a $\mu_1\_\eta^1$: η^1 chelating mode (Scheme 2(b)). In **3**, the pda^{2-} ligand adopts a μ_5-bridging mode with one carboxylate group in a $\mu_2\_\eta^1$: η^1 monodentate mode with a *syn-trans* type and the other in a $\mu_3\_\eta^2$: η^1 mode (Scheme 2(c)). There are two different coordination modes of the pda ligand in **4** (Scheme 2(d) and (e)). In Scheme 2(d), the pda ligand adopts a μ_4-bridging mode with two carboxylate groups in

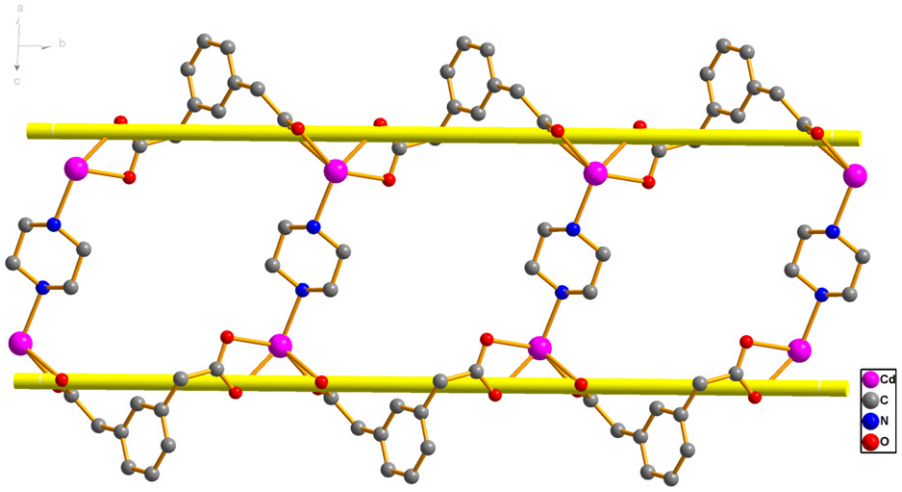

Fig. 4. 1D ladder-like chain structure along *a* axis in **2**.

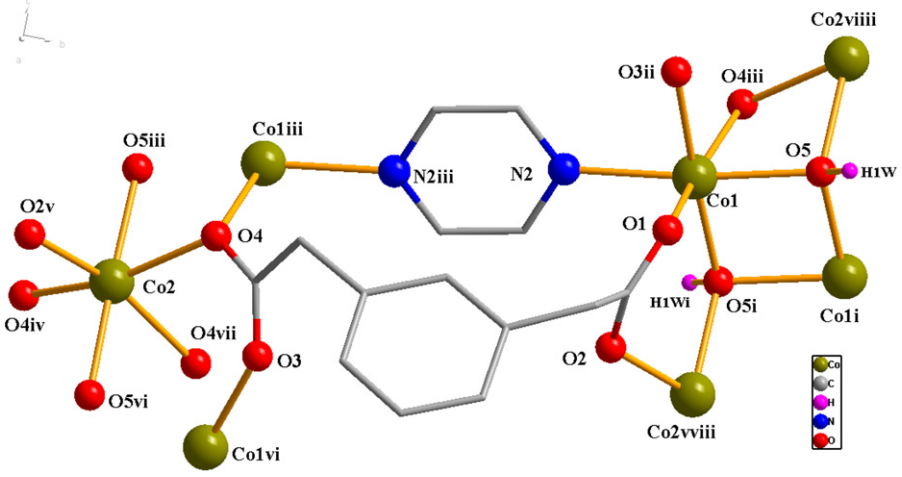

Fig. 5. The coordination environments of Co^{2+}, pda, and pyz in **3** (symmetry code: i, $-x$, $-y+1$, $-z+1$; ii, x, $-y$, $z+1/2$; iii, $-x$, $-y$, $-z+1$; iv, $-x$, $y-1$, $-z+1/2$; v, x, $y-1$, z; vi, x, $-y$, $z-1/2$; vii, $-x$, y, $-z+1/2$; viiii, x, $-y+1$, $z+1/2$; vviii, x, $y+1$, z).

a μ_2_η^2: η^1 mode. As shown in Scheme 2(e), the pda ligand takes a μ_4-bridging mode with one carboxylate group in a μ_2_η^2: η^1 mode and the other in a μ_2_η^1: η^1 monodentate mode with a *syn-trans* type. The results indicate that the pda ligands can have various coordination modes to meet the center metal ions in the compounds.

4.3. Thermal analyses

In order to examine their thermal stabilities and decomposition behavior, the thermal gravimetric analyses (TGA) of complexes **1**–**4** were carried out at the rate of 10 °C/min under nitrogen atmosphere. As shown in Fig. 11, complex **1** undergoes a slow mass loss of 7.8% between 100 and 282 °C, with the loss of one coordinated water molecule and one lattice water molecule (calcd 8.0%). Then the framework is destroyed gradually. Similar to complex **1**, complex **2** also undergoes a slow mass loss of 5.5% between 100 and 201 °C, with the loss of one coordinated water molecule (calcd 4.9%). Then the framework is destroyed gradually. For **3**, the curve exhibits the first weight loss of 5.9% (calcd 5.1%) from 80 to 250 °C, which corresponds to the loss of two water molecules. Then the framework is destroyed gradually. For complex **4**, curve exhibits the first weight loss of 4.9% (calcd 4.0%) from 60 to 250 °C, which corresponds to the loss of two coordinated water molecules. Above 330 °C, the framework is destroyed gradually. The TG results show that the 3D complex **4** is more stable than 1D complexes **1** and **2** and 2D complex **3**.

4.4. X-ray powder diffraction (XRPD) measurement

X-ray powder diffraction (XRPD) was used to confirm the phase purity of bulk materials of compounds **1**–**4** at room temperature (Fig. S7). Although some minor differences can be seen from the experimental patterns compared with those simulated from the single-crystal data, it still indicates that the synthesized materials of compounds **1**–**4** are homogeneous systems.

4.5. Luminescent properties

The d^{10} metal complexes are found to exhibit interesting photoluminescent properties [17,18]. The emissions of H_2pda and both complexes **1** and **2** in the solid state were investigated at room temperature (Fig. 12). The emission of compound **1** is red-shifted relative to that of the free H_2pda ligand, which can be assigned to the ligand-to-metal charge transfer (LMCT) [20]. Complex **2** exhibits intense blue luminescence, which is no shift

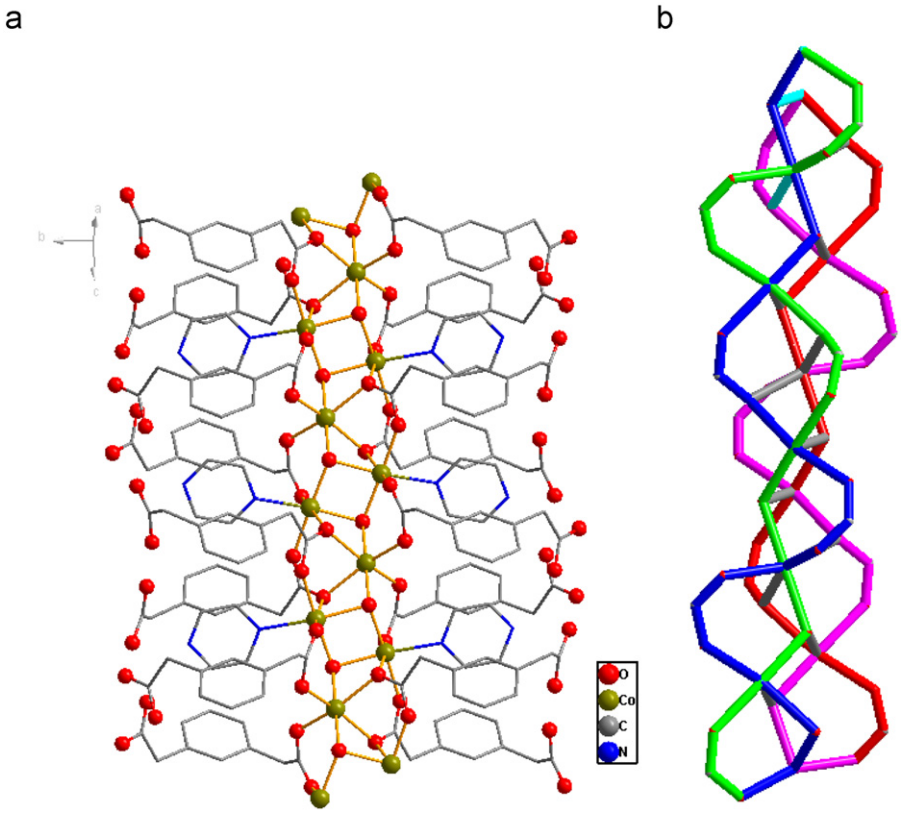

Fig. 6. (a) Pda ligands and μ_3–OH^- groups bridge the Co^{2+} centers to form helix chains in **3**. (b) The representation of two pairs of double-helix chains.

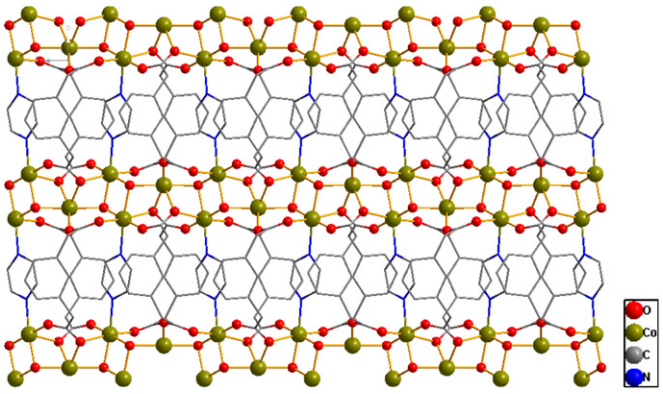

Fig. 7. 2D structure along *a* axis in **3**.

relative to that of the free H_2pda ligand. It may be assigned to intraligand fluorescence emission [21].

4.6. Magnetic properties

The magnetic susceptibility per Co_3 unit measured on a polycrystalline sample of **3** under an applied field of 1000 Oe is shown in Fig. 13. The $\chi_M T$ values at 300 K is 9.21 $cm^3\ mol^{-1}$ K, which is higher than the spin only value of 5.64 $cm^3\ mol^{-1}$ K for magnetically three isolated high-spin Co(II) ($S_{Co}=3/2$, $g=2.0$), owing to the significant orbital contribution of Co(II) in an octahedral environment. Upon cooling, the $\chi_M T$ value drops down very slowly from 9.21 $cm^3\ mol^{-1}$ K at 300 K to a shallow minimum at 38 K and then increases to a value 8.10 $cm^3\ mol^{-1}$ K at 18 K, before dropping to 0.265 $cm^3\ mol^{-1}$ K at 2 K. The Curie–Weiss fit of χ_M^{-1} above 46 K results in a Curie constant $C=9.99\ cm^3\ mol^{-1}$ K and $\theta=-23.9$ K. This large negative θ value indicates not only spin–orbital coupling of the Co(II) ion but also significant antiferromagnetic interactions between the Co(II) ions. The θ value is consistent with those of reported Co(II) compounds with μ_3–OH and carboxylate mixed bridges [22,23]. Since the Co(II) chains in **3** are well separated by the long linkers of pda and pyz bridges, the antiferromagnetic behavior can be suggested to arise from intrachain magnetic interactions of the adjacent trimmers. From the chain structure of **3**, one can get that the main magnetic exchange coupling ways are a typical edge-sharing triangular chain. There are three main magnetic exchange coupling ways: μ_3-hydroxyl, syn–syn and μ_3-carboxylate oxygen atoms of pda, cooperatively contributed by the antiferromagnetic coupling transported by mixed bridges.

The magnetic susceptibility per Pr_2 unit measured on a polycrystalline sample of **4** under an applied field of 1000 Oe is shown in Fig. 14. The $\chi_M T$ value of 2.98 $cm^3\ K\ mol^{-1}$ at room temperature is close to the expected value of 3.20 $cm^3\ K\ mol^{-1}$ for two magnetic isolated Pr(III) ions. Upon lowering the temperature, the $\chi_M T$ value decreases continuously to a value 0.203 $cm^3\ mol^{-1}$ K at 2 K. Between 50 and 300 K, the magnetic susceptibilities can be fitted to the Curie–Weiss law, $\chi_M = C_M/(T-\theta)$, with $C_M=3.43\ cm^3\ mol^{-1}$, $\theta=-46.3$ K. These results indicate a strong antiferromagnetic interactions between the neighboring Pr(III) ions. According to the chain topology, there are only one set of magnetic exchange pathways within the chain: one consists of two μ_2-O bridge from the μ_2-carboxylate groups, cooperatively contributed by the antiferromagnetic coupling transported by mixed bridges, with large Pr–O–Pr (109.2, 111.6°) angles.

5. Conclusions

In summary, four coordination polymers with different architecture have been synthesized by combination the merits of the

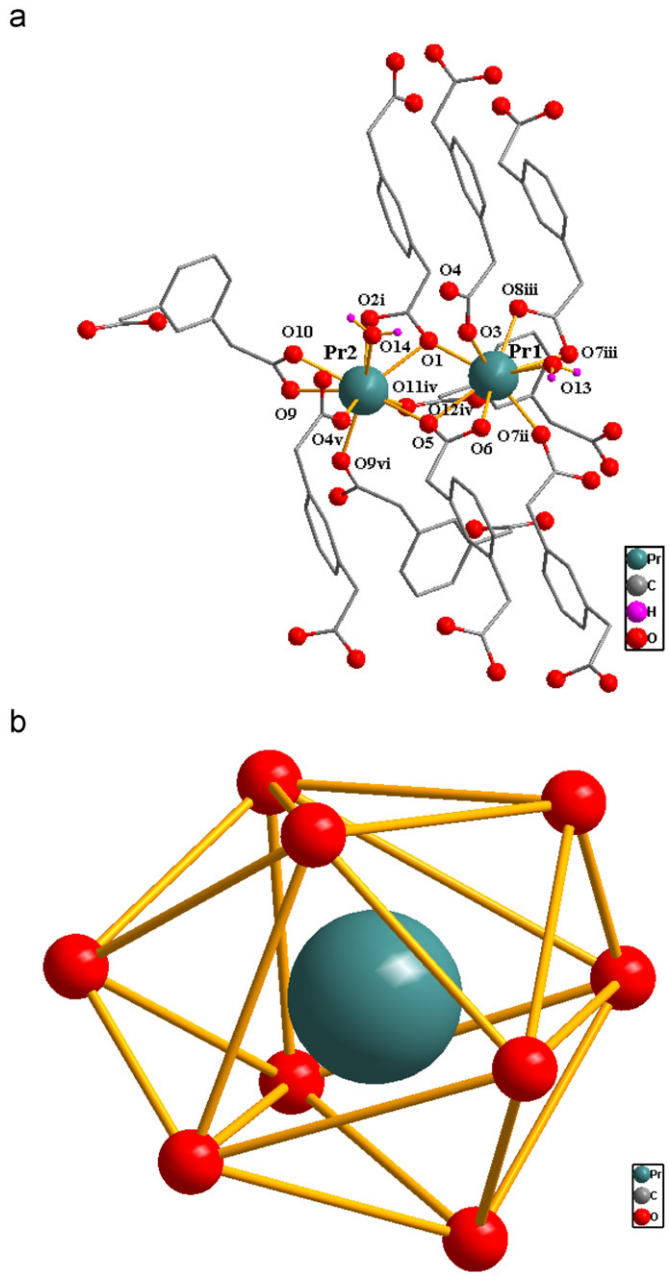

Fig. 8. (a) The coordination environments of Pr^{3+} and pda in **4** (symmetry code: i, $-x+2$, $-y+1$, $-z+2$; ii, $-x+2$, $-y+3$, $-z+3$; iii, x, $y-1$, z; iv, x, y, $z+1$; v, $-x+2$, $-y+2$, $-z+2$; vi, $-x+1$, $-y+2$, $-z+2$.) (b) The distorted tricapped trigonal prism coordination polyhedron of the Pr^{3+} ion of complex **4**.

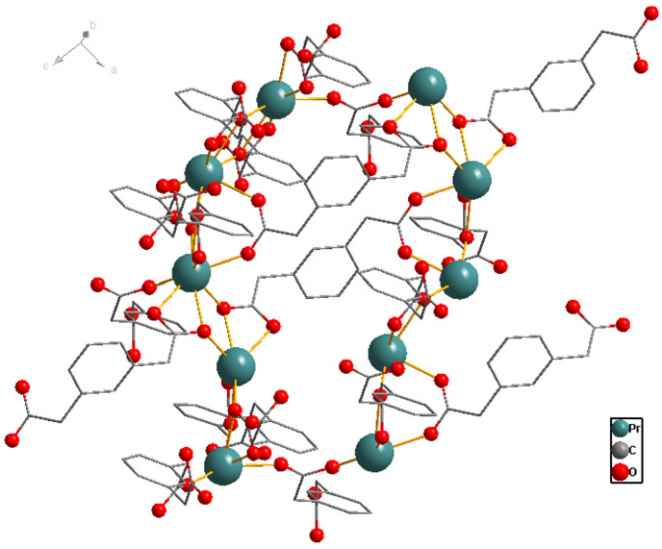

Fig. 9. Eight Pr(III) ions and 12 pda^{2-} ligands form a large $[Pr_8(pda)_{12}]$ ring, and four Pr(III) ions and six pda^{2-} ligands form a small $[Pr_4(pda)_6]$ ring.

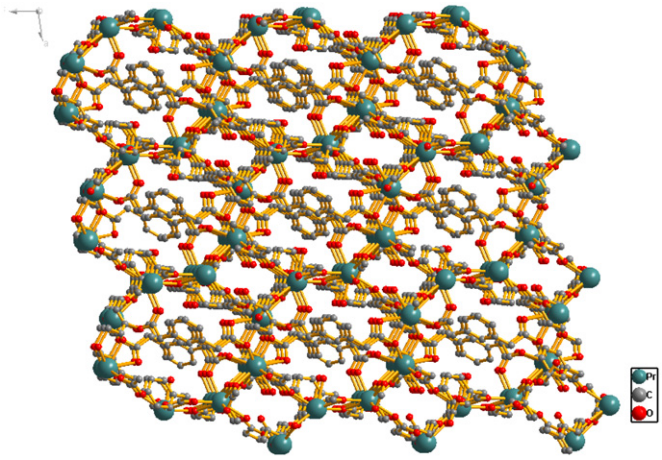

Fig. 10. 3D structure along *b* axis in **4**.

pda ligand, ancillary ligands and different metal ions. This work reveals that the cooperative effect of ligands, ancillary ligands, pH values of the reaction solution and metal ions play a crucial role in resulting structures of the coordination polymers.

Supporting information available

X-ray crystallographic files in CIF format deposited with the Cambridge Structural Databases as files CCDC 783957–783960, respectively, for crystals **1**–**4**. These data can be obtained free of charge via www.ccdc.cam.ac.uk/conts/retrieving.html (or from the Cambridge Crystallographic Data Center, 12 Union Road, Cambridge CB2 1EZ, UK; Fax: (internat.) +441223 336033; E-mail: deposit@ccdc.cam.ac.uk).

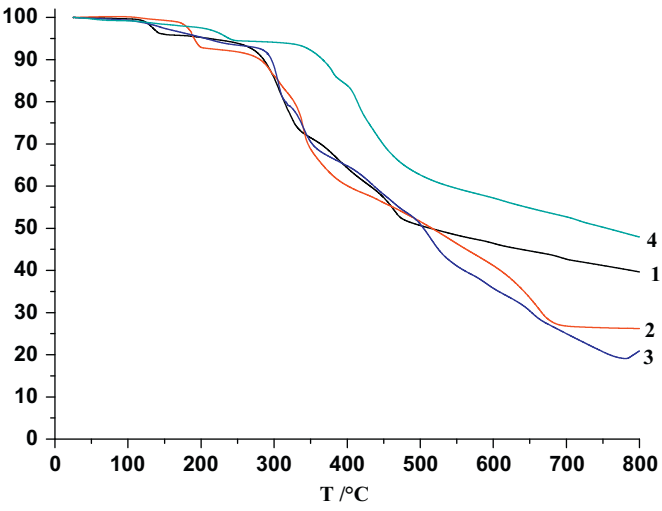

Fig. 11. TG plots of complexes **1**–**4**.

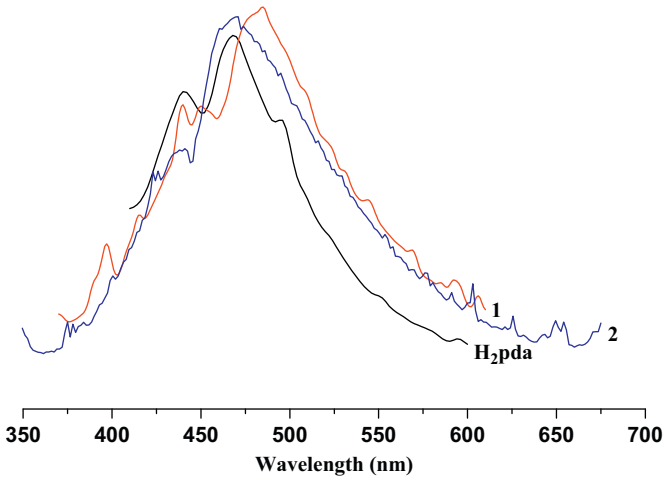

Fig. 12. The emission spectra of **1**, **2**, and H_2pda (λ_{ex}=346 nm, λ_{em}=489 nm for **1**; λ_{ex}=376 nm, λ_{em}=470 nm for **2**; λ_{ex}=377 nm, λ_{em}=470 nm for H_2pda) in the solid state at room temperature.

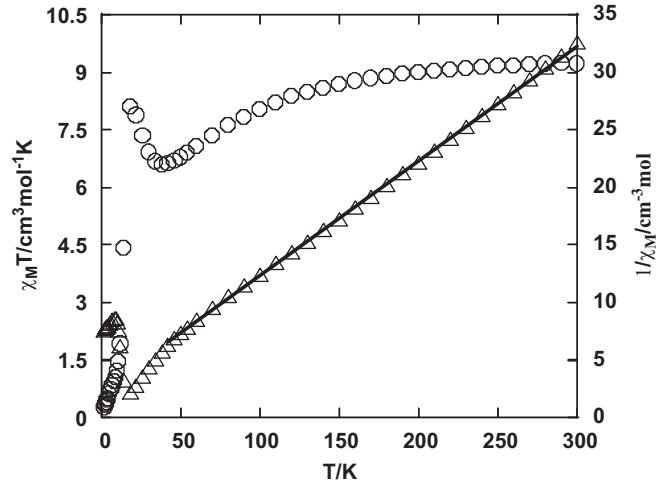

Fig. 13. Temperature dependence of $\chi_M T$ (○) and $1/\chi_M$(□) vs. T for **3**. The black line shows the Curie–Weiss fitting.

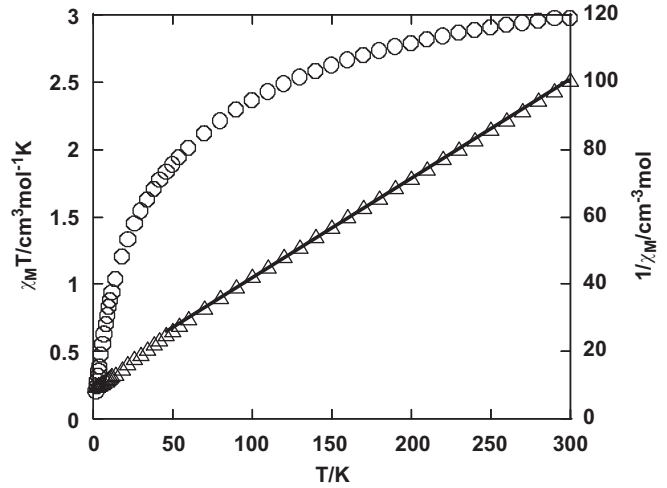

Fig. 14. Temperature dependence of $\chi_M T$ (○) and $1/\chi_M$ (□) vs. T for **4**. The black line shows the Curie–Weiss fitting.

Acknowledgments

This work was supported by the National Natural Science Foundation of China (Project no. 20931003) and the program for New Century Excellent Talents in University (NCET-06-0902). We thank Professor M.H. Zeng for help with the explanation of the magneto-structural correlation.

Appendix A. Supplementary materials

Supplementary data associated with this article can be found in the online version at doi:10.1016/j.jssc.2011.01.030.

References

[1] F. Gándara, A. De Andrés, B. Gómez-Lor, E. Gutiérrez-Puebla, M. Iglesias, M.A. Monge, D.M. Proserpio, N. Snejko, Cryst. Growth Des. 8 (2008) 378–380.
[2] I. Aillaud, J. Collin, C. Duhayon, R. Guillot, D. Lyubov, E. Schulz, A. Trifonov, Chem. Eur. J. 14 (2008) 2189–2200.
[3] L. Pan, K.M. Adams, H.E. Hernandez, X.T. Wang, C. Zheng, Y. Hattori, K. Kaneko, J. Am. Chem. Soc. 125 (2003) 3062–3067.
[4] B.L. Chen, N.W. Ockwig, A.R. Millward, D.S. Contreras, O.M. Yaghi, Angew. Chem. Int. Ed. 44 (2005) 4745–4749.
[5] Z.Y. Li, J.W. Dai, N. Wang, H.H. Qiu, S.T. Yue, Y.L. Liu, Cryst. Growth Des. 10 (2010) 2746–2751.
[6] Y.Z. Zheng, M.L. Tong, W.X. Zhang, X.M. Chen, Angew. Chem. Int. Ed. 45 (2006) 6310–6314.
[7] S.R. Batten, B.F. Hoskins, B. Moubaraki, S. Murray, K.R. Robson, Chem. Commun. (2000) 1095–1096.
[8] S. Kitagawa, R. Kitaura, S.I. Noro, Angew. Chem. Int. Ed. 43 (2004) 2334–2375.
[9] A.Y. Robin, K.M. Fromm, Coord. Chem. Res. 250 (2006) 2127–2158.
[10] X.X. Xu, Y. Lu, E.B. Wang, Y. Ma, X.L. Bai, Cryst. Growth Des. 6 (2006) 2029–2035.
[11] F. Fu, D.S. Li, C.Q. Zhang, J.J. Wang, Y.P. Wu, M. Du, J.W. Wang, Inorg. Chem. Commun. 11 (2008) 1260–1263.
[12] J. Zhou, C.Y. Sun, L.P. Jin, J. Mol. Struct. 832 (2007) 55–62.
[13] Y.G. Huang, F.L. Jiang, D.Q. Yuan, M.Y. Wu, Q. Gao, W. Wei, M.C. Hong, J. Solid State Chem. 182 (2009) 215–222.
[14] G.M. Sheldrick, SADABS, Program for Empirical Absorption Correction of Area Detector Data, University of Göttingen, Göttingen, Germany, 1996.
[15] G.M. Sheldrick, SHELXTL-97, Program for Crystal Structure Solution and Refinement, University of Göttingen, Göttingen, Germany, 1997.
[16] J.Z. Gu, W.G. Lu, L. Jiang, H.C. Zhou, T.B. Lu, Inorg. Chem. 46 (2007) 5835–5837.
[17] G.P. Yang, Y.Y. Wang, W.H. Zhang, A.Y. Fu, R.T. Liu, E.K. Lermontova, Q.Z. Shi, CrystEngComm. 12 (2010) 1509–1517.
[18] W.G. Lu, J.Z. Gu, L. Jiang, M.Y. Tan, T.B. Lu, Cryst. Growth Des. 8 (2008) 192–199.
[19] P. Yang, J.Z. Wu, Y. Yu, Inorg. Chem. Acta 362 (2009) 1907–1912.
[20] Y.Q. Xu, Y.F. Zhou, D.Q. Yuan, M.C. Hong, Chin. J. Struct. Chem. 25 (2006) 704–708.
[21] C.X. Meng, D.S. Li, J. Zhao, F. Fu, X.N. Zhang, L. Tang, Y.Y. Wang, Inorg. Chem. Commun. 12 (2009) 793–795.
[22] M.X. Yao, M.H. Zeng, H.H. Zou, Y.L. Zhou, H. Liang, Dalton Trans. (2008) 2428–2432.
[23] Y.L. Zhou, M.C. Wu, M.H. Zeng, H. Liang, Inorg. Chem. 48 (2009) 10146–10150.